Synthesis and Electrochemical Performance of α-Fe₂O₃ Nano Ellipse as Anode for Lithium-Ion Batteries

Lukman Noerochim[1,*], Eriek Aristya P. Putra[1], Diah Susanti[1],
Firman Mangasa Simanjuntak[1], Tubagus Noor Rohmannudin[1] and Achmad Subhan[2]

[1]Department of Materials Engineering, Sepuluh Nopember Institute of Technology, Surabaya 60111, Indonesia
[2]Research Center of Physics, Indonesian Institute of Science, Serpong, Indonesia

*Corresponding author: E-mail: lukman@mat-eng.its.ac.id

α-Fe₂O₃ with nano ellipse structure was successfully synthesized by one-step hydrothermal method with adding 3, 6, and 9 mmol glycine at 160 °C for 10 h. FE-SEM images present that the shape and size of α-Fe₂O₃ is nano ellipse with dimensions in the range length of 130–200 nm and in the range diameter of 77–120 nm. The as-prepared α-Fe₂O₃ nano ellipse with the addition of glycine by 6 mmol exhibited excellent cycling performance and rate capability when used as anode for lithium ion batteries, obtaining reversible discharge capacity of 206.75 mAh g⁻¹ at 0.3 C. This is attributed to the nano ellipse structure delivering a large particle surface area thus increasing the electric and ionic conductivity of the α-Fe₂O₃ particles as anode. This result demonstrates that α-Fe₂O₃ nano ellipse could be a good candidate as anode material for lithium-ion battery.

Keywords: Glycine, α-Fe₂O₃, Nano ellipse, Hydrothermal, Lithium-ion battery.

INTRODUCTION

In this present era, the demand for lithium-ion battery is increasing rapidly due to the need of various mobile electronic devices such as mobile phones and laptops [1-3]. Even lately, the automotive world has shifted from gasoline car to an electric vehicle that uses lithium-ion battery as a source of their energy [4-6]. This is because the various advantages of lithium batteries such as high capacity, no memory effect, light weight, and more environmentally friendly [7,8]. One component of commercial lithium-ion battery is the anode that is usually fabricated from carbon. Unfortunately, carbon has several disadvantages, namely low theoretical discharge capacity (372 mAh g⁻¹) and the formation of Li dendritic that can cause the long-term of safety [9-11]. In addition, the higher irreversible capacity of carbon that typically appears at the beginning of the charge-discharge profile can cause energy losses. For that it is necessary to obtain electrode material that has a high capacity, durable, higher rate capability, non-toxic, low cost and widespread availability [12,13]. One of the strongest candidates as an anode material is metal oxide because of its

high theoretical capacity, abundant availability, and in terms of safety, it does not give rise to formation of lithium dendrite [14,15].

Various types of metal oxides have been widely investigated for use as anode for lithium-ion batteries such as SnO₂ [16], MoO₃ [17], Mn₃O₄ [18], TiO₂ [19], Fe₃O₄ [20] and α-Fe₂O₃ [21]. α-Fe₂O₃ as the anode is one the promising candidate which there are several advantages such as high theoretical capacity (1007 mAh g⁻¹), low cost, easy fabrication, wide availability and environmental friendly [22,23]. However, there are still some challenges for the practical application as anode materials for α-Fe₂O₃, such as low electronic conductivity and large volume expansion during charge-discharge process which effects on fast capacity fading and poor rate capability. Several strategies are employed to improve the electronic conductivity of α-Fe₂O₃ adding conductive agents such as carbon [24], CNT [25], graphene [26], polyaniline [27] and polypyrrole [28]. However, there are still problems with cycling stability especially in high current densities. To improve the performances of the anode α-Fe₂O₃ especially in terms of stable discharge cycling stability, another of the strategy is by synthesizing

various nano structure of α-Fe$_2$O$_3$, such as nano rod [29], nano tube [30] and nano sphere [31]. In an effort to synthesize α-Fe$_2$O$_3$ nano structure material several techniques are carried out such as ionic liquid-assisted synthesis [32], single-spinneret electrospinning method [33] and reactive spray deposition technology (RSDT) [34]. The previous α-Fe$_2$O$_3$ nanostructure synthesis process is usually a costly procedure and with sacrificial template however severe capacity loss still occurs. Therefore, a feasible and low cost α-Fe$_2$O$_3$ synthesis technique is still required and remained the main target at the moment without sacrificing of the excellent performance of the α-Fe$_2$O$_3$ anode material with a higher specific discharge capacity and enhanced cycling stability.

This work presented the synthesis process of α-Fe$_2$O$_3$ nano ellipse by addition of 3, 6 and 9 mol glycine during hydrothermal process at 160 °C for several hours. Glycine is one type of amino acid which is expected to control hydrolysis process for synthesizing nano structure of α-Fe$_2$O$_3$. The physical characteristic of α-Fe$_2$O$_3$ nano ellipse and electrochemical performance of α-Fe$_2$O$_3$ nano ellipse are presented and studied systematically.

EXPERIMENTAL

α-Fe$_2$O$_3$ with nano ellipse structure was synthesized by hydrothermal method with various content of glycine. Iron(III) chloride hexahydrate (FeCl$_3$·6H$_2$O, Merck, 99.99 %), glycine (Merck, 99.8 %) and ammonia (NH$_4$OH, Merck, 99.99 %) are used as reagent in the synthesizing process of α-Fe$_2$O$_3$ with nano ellipse structure. The experiment is started by dissolving glycine with a size of 3, 6 and 9 mmol mixed with 6 mmol FeCl$_3$·6H$_2$O in 50 mL of deionized water and then stir the mixture with a magnetic stirring until it is completely homogeneous. Each samples were designated as G3, G6 and G9 for 3, 6 and 9 mmol glycine, respectively. Then, 15 mL NH$_4$OH was added to the above solution in a continuously stirred condition. After stirring for 0.5 h, the total solution was transferred into a Teflon-lined stainless steel autoclave and heated at 160 °C for 15 h. Then it is cooled to room temperature, after that the precipitate of the hydrothermal product is washed several times with deionized water and ethanol by centrifugation and after that it was dried in the oven at 100 °C for 24 h. The α-Fe$_2$O$_3$ powder is then characterized by XRD (PANalytical, CuK$_\alpha$ radiation) to analyze the crystal structure and phase, while the particle shape and size are analyzed by FE-SEM (FEI Inspect 250). For electrochemical testing is analyzed by first fabrication of coin cell type CR2032. The α-Fe$_2$O$_3$ nano ellipse is fabricated with in coin cell as a working electrode, lithium metal as a counter and also a reference electrode, for its electrolyte using 1 mol of LiPF6 in diethyl carbonate/ethylene carbonate mixture (1:1 in volume) solution, and Celgard membrane as separator. The fabrication process is carried out in the glove box system (Vigor) under the argon gas with

adjustable levels. The α-Fe$_2$O$_3$ powder is pasted to copper foil by mixing α-Fe$_2$O$_3$ powder by 85 % by weight as the active material, 10 % by weight of acetylene black carbon as additive and 5% by weight of polyvinylidene fluoride (PVDF) as a binder and N-methylpyrrolidone (NMP) as a solvent which all of the materials are mixed homogeneously with agate mortar. The cyclic voltammetry test was performed with an electrochemical work station (WonATech WBCS 2000) with a 0.1 mV/s sweep rate and a potential range of 0.1-3 V. The charge-discharge test coin cells were tested with a recycling battery system (WonATeCH WBCS 2000) with various C - rates from 0.3C to 3C with 5 cycles for each different level. The coin cell impedance is measured with an electrochemical impedance spectroscopy (AutoLab) using frequency of 0.1 - 20,000 Hz and 3V potential.

RESULTS AND DISCUSSION

XRD pattern of the α-Fe$_2$O$_3$ nano ellipse sample in the presence of glycine 3, 6 and 9 mmol at 160 °C for 10 h is shown in Fig. 1. From Fig. 1, it is observed that all samples of α-Fe$_2$O$_3$ synthesized by hydrothermal method indicate as pure hematite (JCPDS card no. 33-0664) [35]. The G9 sample is clearly observed with higher intensity than other samples. This indicates that the G9 sample has a high degree of crysta-linity. All the samples that were successful indexed did not show any impurities, which means that all samples have a high degree of purity. To observe the effect of adding glycine to α-Fe$_2$O$_3$ crystal structure, the size of crytallite size on all samples is calculated at the highest of 2θ on hkl plane (1 0 4) by Debye Scherrer formula as shown at Table-1. It can be seen in Table-1 that the addition of glycine decreases crystallite size with optimum conditions achieved in the addition of 6 mmol glycine with a crystallite size of 41.32 nm. The smaller size of crystallite could induce the grain size of materials that it is very
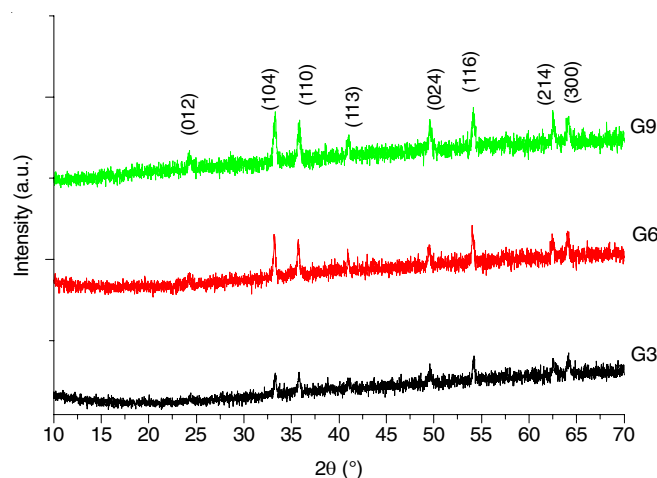

Fig. 1. X-ray diffraction pattern of the α-Fe$_2$O$_3$ sample with the addition of glycine 3 (G3), 6 (G6) and 9 mmol (G9)

TABLE-1
CRYSTALLITE SIZE OF α-Fe$_2$O$_3$ SAMPLE WITH THE ADDITION OF GLYCINE 3 (G3), 6 (G6) AND 9 mmol (G9)

Sample	λ	B	2θ	FWHM	cos θ	D (Å)	D (nm)
G3	1.54056	0.001752	33.345	0.1004	0.958	826.175	82.617
G6	1.54056	0.003502	33.298	0.2007	0.958	413.216	41.322
G9	1.54056	0.002919	33.379	0.1673	0.958	495.819	49.582

influential on the conductivity of the sample [36,37]. Therefore, the effect of glycine on this conductivity will be evaluated by further measurement with electrochemical impedance spectroscopy (EIS).

Field-emission scanning electron microscopy (FE-SEM) images present clearly the microstructure and morphology of the α-Fe_2O_3 nano ellipse sample (Fig. 2). Fig. 2 displays FE-SEM images that the morphology of α-Fe_2O_3 is an ellipse with almost homogeneous size and uniform distribution. Fig. 2(a-c) reveals that the size of α-Fe_2O_3 nanoellipses is in the range
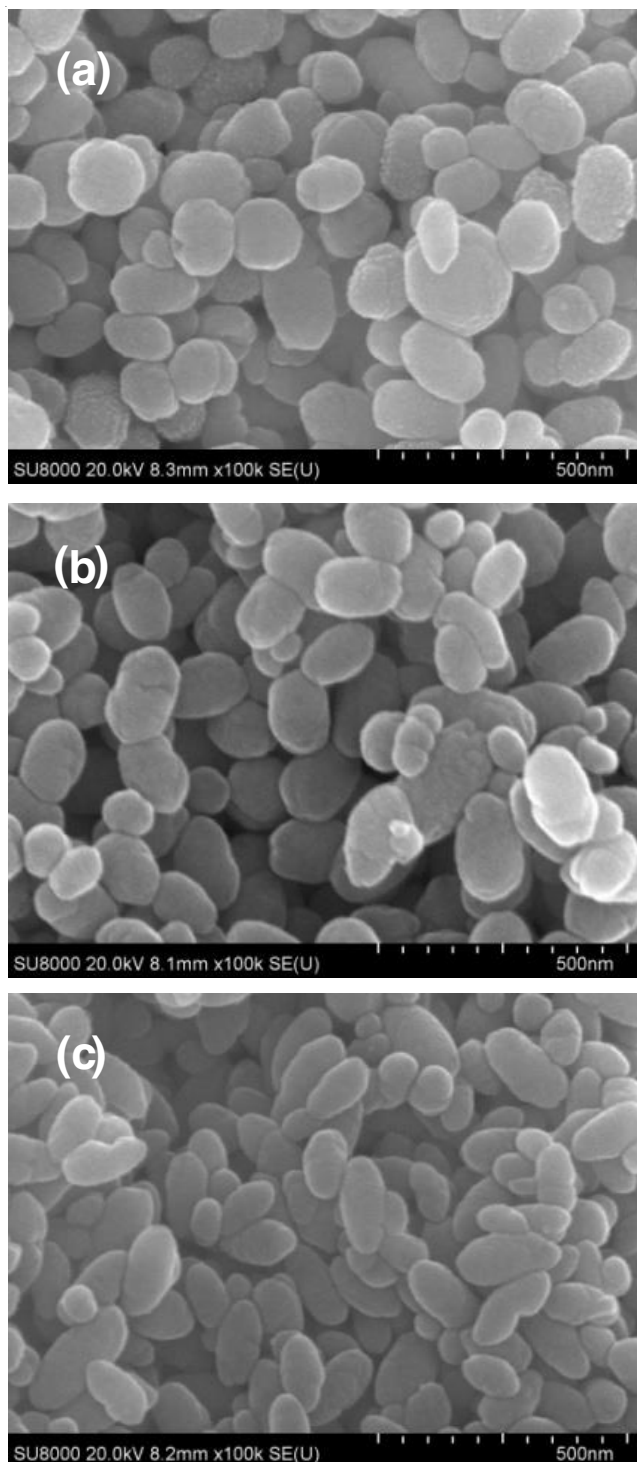

Fig. 2. FE-SEM images of α-Fe_2O_3 show elliptical morphology (a) 3 mmol, (b) 6 mmol and (c) 9 mmol of glycine

length of 130–200 nm and in the range diameter of 77–120 nm. Fig. 2c shows that the increasing content of glycine increased the length of α-Fe_2O_3 grain. The mechanism of the formation of α-Fe_2O_3 nano ellipses might be attributed to the hydrolysis process of $FeCl_3$ connecting to the glycine molecule. Prior to the hydrothermal process, the all precursors of $FeCl_3 \cdot 6H_2O$, glycine and NH_4OH are mixed well in which several reactions could have occurred, such as decomposition, hydrolysis and metal ion complexation [38]. When $FeCl_3 \cdot 6H_2O$ is dissolved in deionized water, it will form a transparent yellow solution. And when glycine is added to the previous solution, then the color turns into a purple black. Most likely this is due to the process of forming compounds between Fe^{3+} ion and glycine. At the beginning of the hydrothermal process, NH_4OH decomposes into NH_3 and H_2O which contribute to the basic condition in the hydrolysis process of Fe^{3+} ion which eventually forms the iron oxide nanocrystals. The $-COO^-$ terminal of glycine is connected with iron oxide nanocrystal. The more glycine are added the more $-COO^-$ terminal of glycine linked to the iron nanocrystal oxide in the nano ellipse formation process. Coupled with the conditions under high temperature and pressure in the autoclave, it further enhances the formation process. It can be concluded here that the glycine is an important factor in the process of nano ellipse formation.

Fig. 3 shows the cyclic voltammograms (CVs) of the α-Fe_2O_3 nano ellipse electrode between 0.1 V and 3 V at a scan rate of 0.5 mV s⁻¹. It can be clearly observed from the first curve of CV that the pair of redox peak is characteristic of α-Fe_2O_3 as reported by previous study [11]. A sharp peak profile of cathodic scan at a potential of 0.5 V attributes to the Li intercalation into α-Fe_2O_3 and the formation of Li_2O. While on the following peak of anodic scan at a potential of 1.7 V is observed the fall in intensity and tend to broaden indicating the irreversible phase transformation in the lithium extraction process in the first cycle. The oxidation peak at a potential of 1.7 V when an anodic scan is a process of change from Fe^0 to Fe^{3+}. In the following cycle after the first cycle, the cathodic peak shows a significant change. The cathodic peak shifted at 1.0 V while the anodic peak remain not change. This might be due to changes in α-Fe_2O_3 nano ellipse after the first reduction reaction process of crystallinity of α-Fe_2O_3 destroyed and cannot survive to continue the subsequent charge-discharge process therefore the α-Fe_2O_3 electrode undergoes changes in electrochemical behavior such as amorphous α-Fe_2O_3 as reported by Liu *et al.* [39]. In the subsequent cycles after first cycle, the peaks exhibit little change, suggesting good stability during Li-ion insertion and extraction process.

Fig. 4 shows the high rate discharge-charge curve of the α-Fe_2O_3 nanoellipse electrode with 3, 6 and 9 mmol glycine, respectively. All discharge-charge curves have the same features as α-Fe_2O_3 reported by Wang *et al.* [31]. For the case of α-Fe_2O_3 with 6 mmol (Fig. 4b), it can be clearly observed that around 1.0 V the first profile of the discharge curve is inclining with a long slope, in good agreement with the CV curves profile. While the charge curve shows a sloping plateau at ~1.7 V due to the Li extraction process. The first reaction process contributes a specific discharge capacity of 206.75 mAh g⁻¹ for α-Fe_2O_3 with 6 mmol electrode. The later process
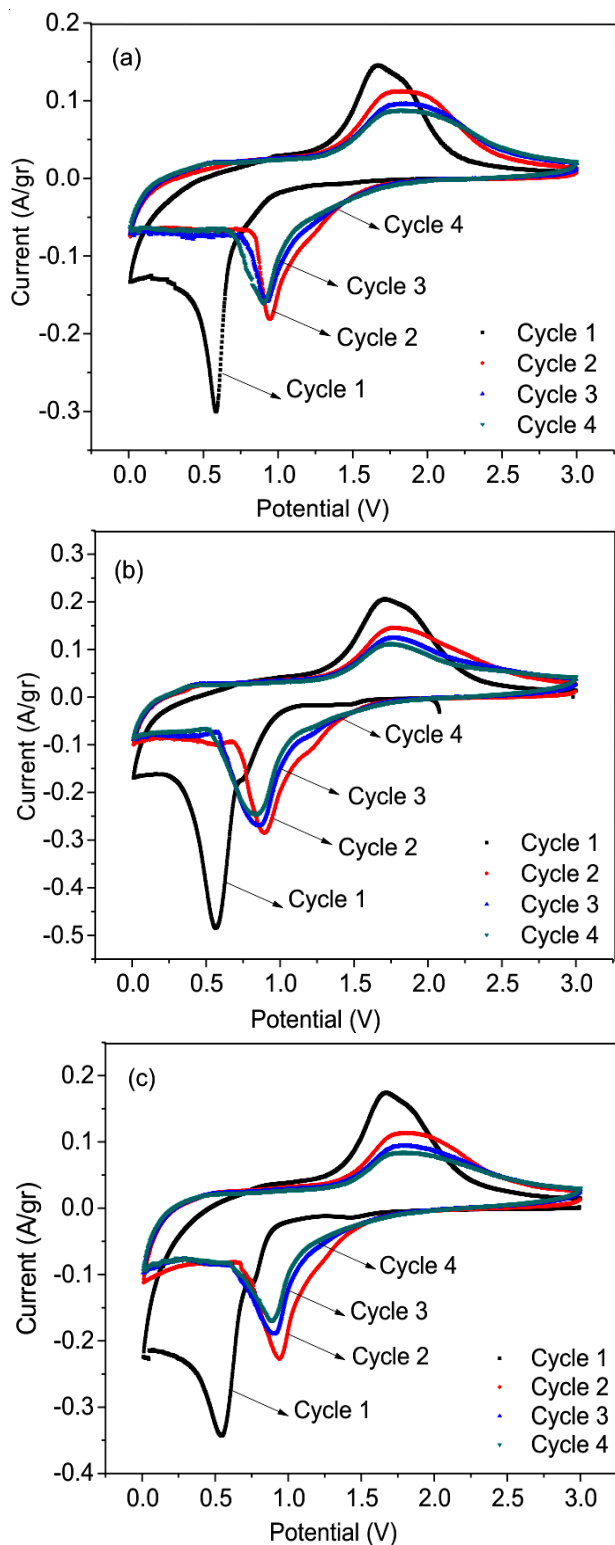
Fig. 3. Cyclic voltammograms (CVs) of the elliptical α-Fe₂O₃ electrode between 0.1 V and 3 V at a scan rate of 0.5 mV s⁻¹ (a) 3 mmol, (b) 6 mmol and (c) 9 mmol of glycine

Fig. 4. High rate discharge/charge curve of α-Fe₂O₃ nanoellipse electrode (a) 3 mmol, (b) 6 mmol and (c) 9 mmol of glycine

deliveries a reversible charge capacity of 161.23 mAh g⁻¹, so the value of capacity loss is found about 21 %. The specific discharge capacities of the elliptical α-Fe₂O₃ electrode at about 206.75 mAh g⁻¹ when cycled at 0.3C , 138.32 mAh g⁻¹ at 1C and finally at the last rate giving capacity 65.66 mAh g⁻¹ at 3C, all of which are higher than other samples as shown in Fig. 4(b). The detail discharge capacity at high rate for all α-Fe₂O₃
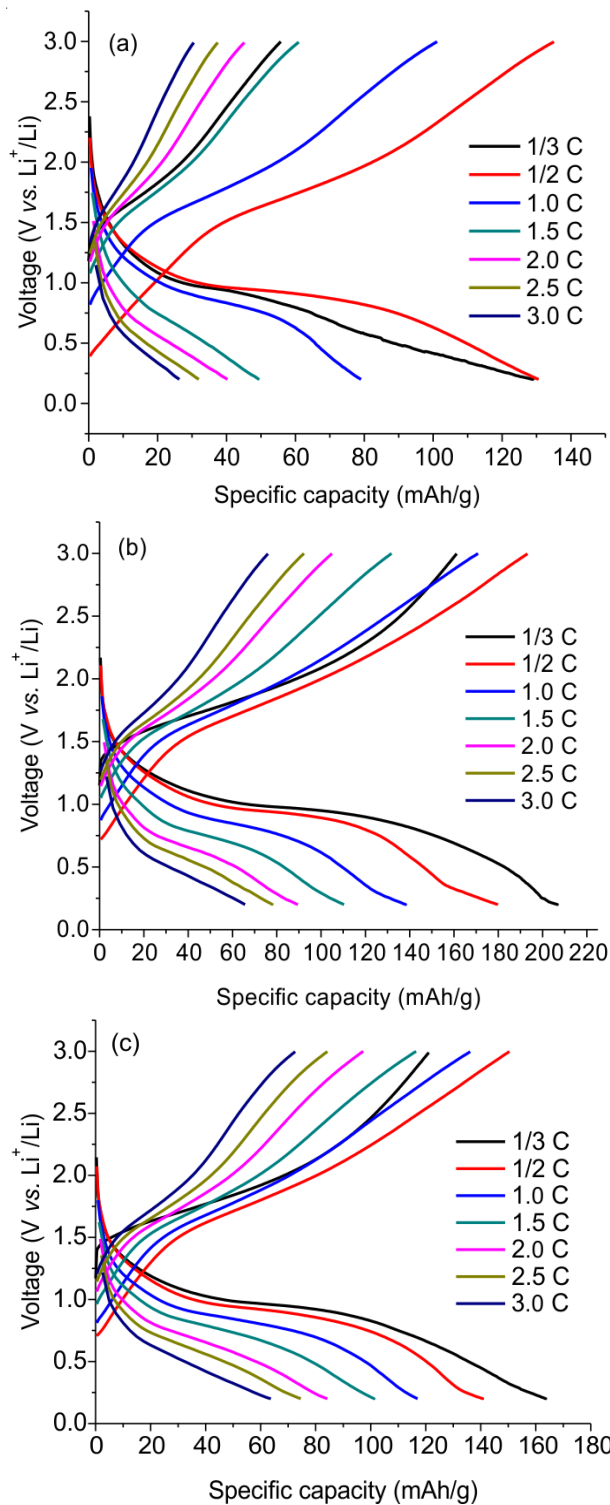
samples is presented in Table-2. It reveals that G6 sample has a good redox reaction process involving lithium ion diffusion into the particle.

Fig. 5 shows the electrochemical impedance spectroscopy (EIS) of the α-Fe₂O₃ nanoellipse electrode in order to further analyze the bulk resistance and Li-ion diffusion. The equivalent circuit for the modeling of the Nyquist plot is shown in insert Fig. 5 as reported by Liu *et al.* [40]. R_e is the internal resistance of the battery cell, R_{ct} represents the charge-transfer resistance

TABLE-2
SELECTED SPECIFIC DISCHARGE CAPACITY OF ALL α-Fe$_2$O$_3$ SAMPLES AT DIFFERENT C-RATE

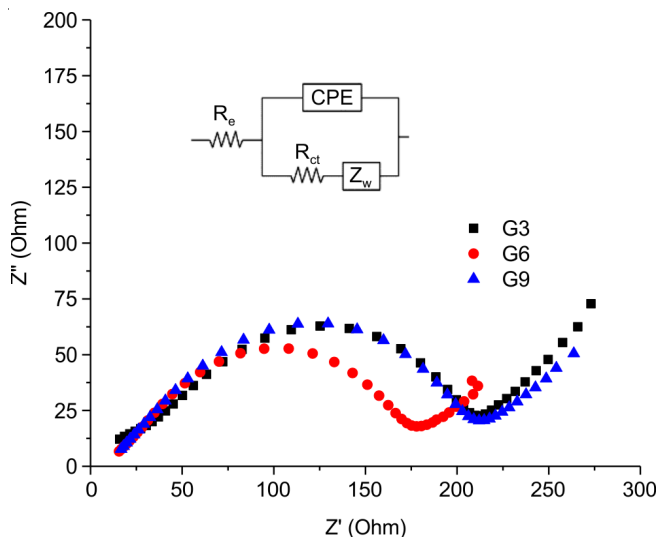| Sample	Specific discharge capacity (mAh/g)						
	0.3C	0.5C	1.0C	1.5C	2.0C	2.5C	3.0C
G3	129.32	130.11	79.23	49.35	40.21	31.54	26.12
G6	206.75	179.56	138.32	110.76	89.43	78.23	65.66
G9	163.23	140.16	117.56	101.27	84.36	74.17	63.33

Fig. 5.   Nyquist plot of α-Fe$_2$O$_3$ nano ellipse electrode for 3 mmol, 6 mmol and 9 mmol of glycine, respectively

and CPE is associated with and constant phase element of the electrode/electrolyte interface. While Z_w is chosen to represent the bulk diffusion of lithium ions. It can be seen that the charge-transfer resistance R_{ct} of the α-Fe$_2$O$_3$ nano ellipse electrode with the 6 mmol glycine is 177 Ω, that are significantly lower than the α-Fe$_2$O$_3$ nano ellipses with 3 and 9 mmol glycine (215 and 212 Ω). This fact shows that after the cycling process, the electrons move more easily in the α-Fe$_2$O$_3$ nano ellipses with 6 mmol glycine. This demonstrates that adding glycine at the accurate amount enhances the surface area of the α-Fe$_2$O$_3$ nano ellipses which is increasing ionic conductivity of the active materials and decreasing the resistance. Finally, α-Fe$_2$O$_3$ nano ellipse electrode with 6 mmol glycine posses high reversible capacity and high-rate capability, would be a material alternative for anode materials of lithium batteries.

Conclusion

The elliptical grains of α-Fe$_2$O$_3$ were successfully synthesized by a simple hydrothermal method in the presence of glycine. FE-SEM images show that the concentration of glycine increases the length of the grain. The as-prepared α-Fe$_2$O$_3$ nanoellipse has dimensions in the range length of 130–200 nm and in the range diameter of 77–120 nm. When evaluated as an anode material in the high rate cycles, the α-Fe$_2$O$_3$ nano-ellipse anode material with 6 mmol glycine shows the highest discharge capacity of about 206.75 mAh g^{-1} at 0.3C and 65.66 mAh g^{-1} at 3C. This work demonstrates that adding glycine at the accurate amount enhances the surface area of the α-Fe$_2$O$_3$ nano ellipses which is increasing ionic conductivity of the active materials and decreasing the resistance. The α-Fe$_2$O$_3$ nano-ellipse anode material with 6 mmol glycine has good lithium storage performance as potential anode for lithium-ion battery.

CONFLICT OF INTEREST

The authors declare that there is no conflict of interests regarding the publication of this article.

REFERENCES

1. P. Poizot, S. Laruelle, S. Grugeon, L. Dupont and J.-M. Tarascon, *Nature*, **407**, 496 (2000);
https://doi.org/10.1038/35035045.
2. Z. Li, L. Li, W. Zhong, A. Cheng, W. Fu, Z. Li and H. Zhang, *J. Alloys Compd.*, **766**, 253 (2018);
https://doi.org/10.1016/j.jallcom.2018.06.316.
3. P. Roy and S.K. Srivastava, *J. Mater. Chem. A Mater. Energy Sustain.*, **3**, 2454 (2015);
https://doi.org/10.1039/C4TA04980B.
4. M.N. Obrovac and V.L. Chevrier, *Chem. Rev.*, **114**, 11444 (2014);
https://doi.org/10.1021/cr500207g.
5. W. Guanghui, L. Ruiyi, L. Zaijun, L. Junkang, G. Zhiguo and W. Guangli, *Electrochim. Acta*, **171**, 156 (2015);
https://doi.org/10.1016/j.electacta.2015.05.016.
6. S. Zhu, J. Li, X. Deng, C. He, E. Liu, F. He, C. Shi and N. Zhao, *Adv. Funct. Mater.*, **27**, 1605017 (2017);
https://doi.org/10.1002/adfm.201605017.
7. Y. Gu, F. Wu and Y. Wang, *Adv. Funct. Mater.*, **23**, 893 (2013);
https://doi.org/10.1002/adfm.201202136.
8. Z. Wang, Z. Wang, W. Liu, W. Xiao and X.W.D. Lou, *Energy Environ. Sci.*, **6**, 87 (2013);
https://doi.org/10.1039/C2EE23330D.
9. C. Li, Z. Li, X. Ye, X. Yang, G. Zhang and Z. Li, *Chem. Eng. J.*, **334**, 1614 (2018);
https://doi.org/10.1016/j.cej.2017.11.142.
10. S. Xu, C.M. Hessel, H. Ren, R. Yu, Q. Jin, M. Yang, H. Zhao and D. Wang, *Energy Environ. Sci.*, **7**, 632 (2014);
https://doi.org/10.1039/C3EE43319F.
11. F. Zhou, S. Xin, H.-W. Liang, L.-T. Song and S.-H. Yu, *Angew. Chem. Int. Ed.*, **53**, 11552 (2014);
https://doi.org/10.1002/anie.201407103.
12. X. Zhu, Y. Zhu, S. Murali, M.D. Stoller and R.S. Ruoff, *ACS Nano*, **5**, 3333 (2011);
https://doi.org/10.1021/nn200493r.
13. Y. Sun, X. Hu, W. Luo and Y. Huang, *ACS Nano*, **5**, 7100 (2011);
https://doi.org/10.1021/nn201802c.
14. Z. Wang, S. Madhavi and X. Wen (David) Lou, *J. Phys. Chem. C*, **116**, 12508 (2012);
https://doi.org/10.1021/jp304216z.
15. H.B. Wu, J.S. Chen, H.H. Hng and X. Wen (David) Lou, *Nanoscale*, **4**, 2526 (2012);
https://doi.org/10.1039/c2nr11966h.
16. K. Kravchyk, L. Protesescu, M.I. Bodnarchuk, F. Krumeich, M. Yarema, M. Walter, C. Guntlin and M.V. Kovalenko, *J. Am. Chem. Soc.*, **135**, 4199 (2013);
https://doi.org/10.1021/ja312604r.
17. T. Tao, A.M. Glushenkov, C. Zhang, H. Zhang, D. Zhou, Z. Guo, H.K. Liu, Q. Chen, H. Hu and Y. Chen, *J. Mater. Chem.*, **21**, 9350 (2011);
https://doi.org/10.1039/c1jm10220f.

18. H. Wang, L.-F. Cui, Y. Yang, H. Sanchez Casalongue, J.T. Robinson, Y. Liang, Y. Cui and H. Dai, *J. Am. Chem. Soc.*, **132**, 13978 (2010); https://doi.org/10.1021/ja105296a.

19. J. Qu, Q.-D. Wu, Y.-R. Ren, Z. Su, C. Lai and J.-N. Ding, *Chem. Asian J.*, **7**, 2516 (2012); https://doi.org/10.1002/asia.201200551.

20. Y. Chen, H. Xia, L. Lu and J. Xue, *J. Mater. Chem.*, **22**, 5006 (2012); https://doi.org/10.1039/c2jm15440d.

21. X. Wang, Y. Xiao, C. Hu and M. Cao, *Mater. Res. Bull.*, **59**, 162 (2014); https://doi.org/10.1016/j.materresbull.2014.07.008.

22. Z. Wang, D. Luan, S. Madhavi, Y. Hu and X. Wen (David) Lou, *Energy Environ. Sci.*, **5**, 5252 (2012); https://doi.org/10.1039/C1EE02831F.

23. X.-L. Wu, Y.-G. Guo, L.-J. Wan and C.-W. Hu, *J. Phys. Chem. C*, **112**, 16824 (2008); https://doi.org/10.1021/jp8058307.

24. R. Liu, C. Zhang, Q. Wang, C. Shen, Y. Wang, Y. Dong, N. Zhang and M. Wu, *J. Alloys Compd.*, **742**, 490 (2018); https://doi.org/10.1016/j.jallcom.2018.01.262.

25. M. Wu, J. Chen, C. Wang, F. Wang, B. Yi, W. Su, Z. Wei and S. Liu, *Electrochim. Acta*, **132**, 533 (2014); https://doi.org/10.1016/j.electacta.2014.04.032.

26. J. Wang, L. Lin and D. He, *J. Alloys Compd.*, **750**, 871 (2018); https://doi.org/10.1016/j.jallcom.2018.04.079.

27. J. Guo, L. Chen, G. Wang, X. Zhang and F. Li, *J. Power Sources*, **246**, 862 (2014); https://doi.org/10.1016/j.jpowsour.2013.08.052.

28. J. Liu, W. Zhou, L. Lai, H. Yang, S. Hua Lim, Y. Zhen, T. Yu, Z. Shen and J. Lin, *Nano Energy*, **2**, 726 (2013); https://doi.org/10.1016/j.nanoen.2012.12.008.

29. Y.-M. Lin, P.R. Abel, A. Heller and C.B. Mullins, *J. Phys. Chem. Lett.*, **2**, 2885 (2011); https://doi.org/10.1021/jz201363j.

30. J. Chen, L. Xu, W. Li and X. Gou, *Adv. Mater.*, **17**, 582 (2005); https://doi.org/10.1002/adma.200401101.

31. B. Wang, J.S. Chen, H.B. Wu, Z. Wang and X.W.D. Lou, *J. Am. Chem. Soc.*, **133**, 17146 (2011); https://doi.org/10.1021/ja208346s.

32. J. Lian, X. Duan, J. Ma, P. Peng, T. Kim and W. Zheng, *ACS Nano*, **3**, 3749 (2009); https://doi.org/10.1021/nn900941e.

33. H. Wang, Y. Zhou, Y. Shen, Y. Li, Q. Zuo and Q. Duan, *Electrochim. Acta*, **158**, 105 (2015); https://doi.org/10.1016/j.electacta.2015.01.149.

34. Y. Wang, J. Roller and R. Maric, *J. Power Sources*, **378**, 511 (2018); https://doi.org/10.1016/j.jpowsour.2017.12.047.

35. X. Hu, J.C. Yu, J. Gong, Q. Li and G. Li, *Adv. Mater.*, **19**, 2324 (2007); https://doi.org/10.1002/adma.200602176.

36. S.F. Abbas, S.-J. Seo, K.-T. Park, B.-S. Kim and T.-S. Kim, *J. Alloys Compd.*, **720**, 8 (2017); https://doi.org/10.1016/j.jallcom.2017.05.244.

37. A.I. Ioffe, M.V. Inozemtsev, A.S. Lipilin, M.V. Perfilev and S.V. Karpachov, *Phys. Status Solidi*, **30**, 87 (1975); https://doi.org/10.1002/pssa.2210300109.

38. H. Chen, Y. Zhao, M. Yang, J. He, P.K. Chu, J. Zhang and S. Wu, *Anal. Chim. Acta*, **659**, 266 (2010); https://doi.org/10.1016/j.aca.2009.11.040.

39. X. Liu, W. Si, J. Zhang, X. Sun, J. Deng, S. Baunack, S. Oswald, L. Liu, C. Yan and O.G. Schmidt, *Sci. Rep.*, **4**, 7452 (2015); https://doi.org/10.1038/srep07452.

40. H. Liu, G. Wang, J. Wang and D. Wexler, *Electrochem. Commun.*, **10**, 1879 (2008); https://doi.org/10.1016/j.elecom.2008.09.036.